

SPECTROPHOTOMETRIC DETECTION OF URIC ACID WITH ENZYME-LIKE REACTION MEDIATED 3,3',5,5'-TETRAMETHYLBENZIDINE OXIDATION

Jin Yang, Shi Qi Cheng, Rui Shi, Shang Ying Qin, Li Huang and Yi Lin Wang*

School of Chemistry and Chemical Engineering, Guangxi Key Laboratory of Electrochemical Energy Materials, Guangxi University, Nanning 530004, China

(Received April 27, 2022; Revised August 8, 2022; Accepted August 9, 2022)

ABSTRACT. WO₃ nanosheets (NSs) were prepared and characterized by X-ray photoelectron spectrometer (XPS), X-ray diffractometer (XRD), scanning electron microscope (SEM) and transmission electron microscope (TEM). The obtained WO₃ NSs exhibited peroxidase-like catalytic activity, which can catalyze H₂O₂ to oxidize 3,3',5,5'-tetramethylbenzidine (TMB) to generate oxidized TMB (oxTMB) with an absorption peak centered at 652 nm. Based on this, a facile method for the spectrophotometric determination of H₂O₂ was established. Under the selected conditions, the increase in absorbance of oxTMB enabled the detection of H₂O₂ ranging from 2.0 to 180 μM. Considering the fact that H₂O₂ is one of the products of urate oxidase (UAO)-catalyzed uric acid (UA) oxidation, a convenient method for the selective determination of UA was further developed with the help of UV-Vis spectrophotometer. The increase of absorbance at 652 nm showed a linear response to UA concentration over the range of 2.0–180 μM. The limit of detection for UA was as low as 1.25 μM. More importantly, the proposed method was applied to the determination of UA in serum samples with satisfactory results.

KEY WORDS: Spectrophotometric, WO₃ nanosheets, Uric acid, Determination

INTRODUCTION

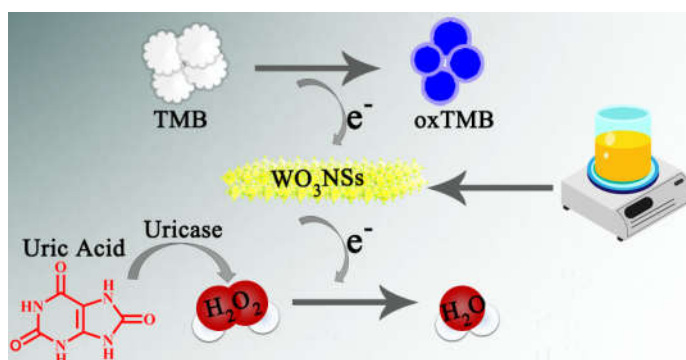
Uric acid (UA), the end product of purine metabolism, is one of the main antioxidants in human body, which can be detected in serum and urine [1, 2]. When the serum UA content exceeds 0.46 mM [2], it is considered to be high UA, which is identified as to be a risk signal for various diseases [3] including cardiovascular disease, kidney disease and metabolic syndrome [4-6]. On the contrary, a low level (below 0.12 mM) of UA in human blood indicates signs of Parkinson's disease or multiple sclerosis [4, 5]. Therefore, accurate determination of UA in serum is of great importance for disease diagnosis. So far, different analysis techniques have been used for the detection of UA in biological samples, including fluorescence [7, 8], high-performance liquid chromatography (HPLC) [9, 10], electrochemical [11] and so on. It is worth noting that fluorescence and HPLC require expensive instruments. Electrochemical method faces complicated electrode modification process. Compared with these methods, colorimetry possesses the advantages of simplicity, rapidity and practicality. It can be used to determine analytes with naked eyes or UV-Vis spectrometer [12-15]. Horseradish peroxidase (HRP) was used in the traditional colorimetry for the determination of H₂O₂ and its related substances such as glucose and UA [16, 17]. Although HRP has the advantages of high catalytic activity and strong specificity, its disadvantages of high cost and poor stability hinder its wide applications [14, 18].

In recent years, seeking substitutes for natural enzymes has attracted extensive attention. In 2007, it was found for the first time that Fe₃O₄ nanoparticles (NPs) could catalyze H₂O₂ to oxidize 3,3',5,5'-tetramethylbenzidine (TMB) [19]. That is, Fe₃O₄ NPs can be used as peroxidase mimetic. This innovative application inspired the research of using nanomaterials as mimic enzymes. Since then, lots of nanomaterials have been reported to exhibit peroxidase (or oxidase)-like activity, including noble metals (e.g. Au@Ag NPs [20], AgNPs@ZnMOF [21], and Ni-Pt NPs [22]), transition metal oxides or sulfides (e.g. MnO₂ NSs [23], CuO NFs [24], CeO₂ NPs [25], and MoS₂

*Corresponding author. E-mail: theanalyst@163.com

This work is licensed under the Creative Commons Attribution 4.0 International License

NSs [26]), carbon-based nanomaterials (e.g. CQDs [27] and GQDs [28]), etc. As a typical transition metal oxide, WO_3 nanomaterials has advantages of high catalytic activity and good chemical stability. Huang's group established a colorimetric sensing platform for H_2O_2 , ascorbic acid and dopamine detection based on WO_3 nanowires (NWs) with peroxidase-like activity [29]. As a peroxidase mimetic, WO_3 quantum dots (QDs) have been applied to construct cholesterol colorimetric sensor [30]. Because of its excellent peroxidase activity, WO_3 nanosheets (NSs) were also applied for the colorimetric determination of xanthine [31]. In the present study, WO_3 NSs were prepared from $\text{Na}_2\text{WO}_4 \cdot 2\text{H}_2\text{O}$ and HNO_3 at room temperature. Based on the peroxidase-like activity of the WO_3 NSs and urate oxidase (UAO)-catalyzed uric acid (UA) oxidation, a convenient and selective colorimetric method was developed for the sensitive detection of UA (Scheme 1).



Scheme 1. Schematic diagram of WO_3 NSs preparation and uric acid determination.

EXPERIMENTAL

Reagents and apparatus

Sodium tungstate ($\text{Na}_2\text{WO}_4 \cdot 2\text{H}_2\text{O}$), hydrogen peroxide (H_2O_2), 3,3',5,5'-tetramethylbenzidine (TMB), isopropanol (IPA) and methanol (MA) were provided by Tianjin Da Mao Chemical Reagent Factory (Tianjin, China). Uric acid (UA), urate oxidase (UAO), glucose (Glu), fructose (Fru), lysine (Lys), threonine (Thr), lactose (Lac) and glycine (Gly) were purchased from Shanghai Maclean Biochemical Co., Ltd, China. Other reagents used in the experiments were from Sinopharm Chemical Reagent Co., Ltd.

The morphology characterizations of WO_3 NSs were performed on a S-3400N scanning electron microscope (SEM) and a Tecnai G2 F20 S-TWIN transmission electron microscope (TEM), respectively. A Bruker D8 X-ray diffractometer (XRD) and an ESCALAB 250Xi X-ray photoelectron spectrometer (XPS) were used for recording XRD and XPS spectra, respectively. A Unico 4802 UV-Vis spectrophotometer was used to measure absorption spectra.

Preparation of WO_3 NSs

WO_3 NSs were prepared using a method from literature with some modification [32]. 0.4 g of $\text{Na}_2\text{WO}_4 \cdot 2\text{H}_2\text{O}$ was dispersed in 300 mL of HNO_3 (4.8 M) while stirring. After 10 min of sonicate, the mixture was subjected to magnetic stirring at room temperature for 72 h. The yellow product was then gathered after centrifugal separation (8000 rpm, 20 min) and followed by washing with ultrapure water. After drying in a 50 °C vacuum oven for 12 h, the obtained yellow solid was

stored in a desiccator. Before used, the WO_3 NSs were ground into fine powder with an agate mortar. 50 mg of powder was taken and dispersed into 50 mL ultrapure water following by sonicate for 2 h.

Detection of H_2O_2 and UA

Aliquots of 200 μL TMB (10 mM) and 50 μL WO_3 NSs (1 mg/mL) were mixed with 200 μL H_2O_2 with different concentration. 1560 μL HAc-NaAc buffer (0.2 M, pH = 4.5) was then added into the above solution. After full mixing, it was incubated in a 30 °C water bath for 50 min. Finally, the absorption spectrum of the resultant solution was recorded.

Both UA and UAO solutions were prepared in Tris buffer (0.1 M, pH = 8.0). The UA detection was carried out as follows: 100 μL UA with different concentration was incubated with 100 μL UAO (1 mg/mL) at 37 °C for 25 min to generate H_2O_2 . Then, 200 μL TMB (10 mM), 50 μL WO_3 NSs (1 mg/mL) and 1560 μL HAc-NaAc buffer (0.2 M, pH = 4.5) were added successively. After fully mixing, it was incubated at 30 °C for another 50 min. Then, the absorption spectrum of the resultant solution was recorded.

The absorbance at 652 nm was applied to establish the calibration curves for H_2O_2 and UA. All experiments were carried out in parallel three times.

Pre-treatment of serum sample

The serum samples from healthy adults were provided by volunteers of our research group and extracted by Guangxi University Affiliated Hospital (Nanning China). A certain amount of serum sample was fully mixed with trichloroacetic acid (10%), it was then centrifuged at 5000 rpm for 20 min to remove serum protein. The collected supernatant was diluted with Tris buffer (0.1 M, pH = 8.0). For standard addition recovery measurement, a certain amount of UA was spiked into the pretreated sample. The determination of UA was performed according to the procedure described in Section 1.3.

RESULTS AND DISCUSSION

Composition and morphology of WO_3 NSs

The chemical composition and crystal structure of WO_3 NSs were identified by XPS and XRD, respectively. As shown in Figure 1A, the existence of W, O, and C elements can be demonstrated in the XPS survey spectra of WO_3 NSs. The C element was most likely to come from the absorption of CO_2 during the measurement. As can be seen in Figure 1B, the binding energy values of $\text{W}4f_{7/2}$ and $\text{W}4f_{5/2}$ are observed at 35.23 and 37.15 eV, respectively, which is consistent with the XPS results of WO_3 in the literature [33]. Suggesting the typical characteristic of W^{6+} oxidation state. The $\text{O}1s$ peak (Figure 1C) at 530.4 eV indicates the existence of O^{2-} in WO_3 . The other $\text{O}1s$ peaks located at 532.7 eV reveals the presence of adsorbed water molecules on the surface of WO_3 [34]. Figure 1D shows the XRD pattern obtained from WO_3 NSs powder. Four characteristic diffraction signals are observed at 16.3°, 24.4°, 25.9°, and 34.4°, which belong to the (001), (110), (011), and (002) crystal planes of WO_3 (JCPDA No.54-0508), respectively. Implying that WO_3 existed in its crystalline form. An obvious lamellar structure can be observed in SEM (Figure 1E) and TEM (Figure 1F) images, indicating that the sample was nanosheets. All these demonstrated the formation of WO_3 NSs.

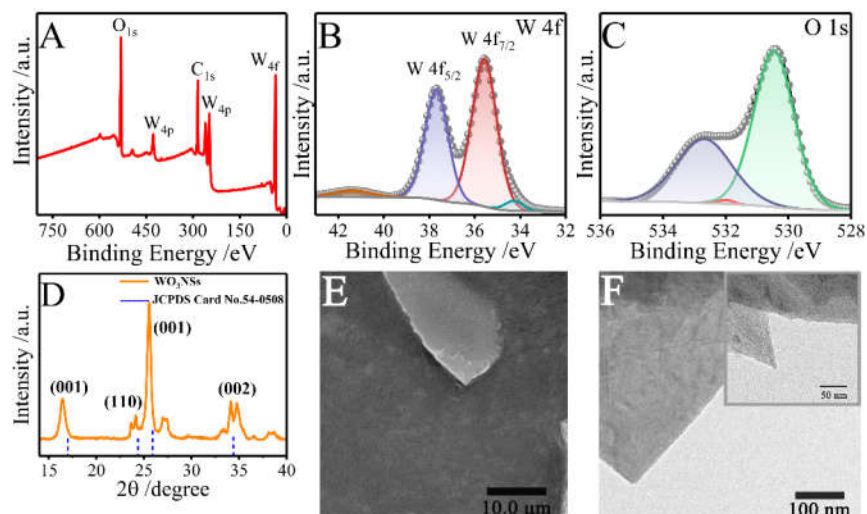


Figure 1. Characterization of WO_3 NSs: (A). The XPS pattern of WO_3 NSs, (B). The XPS pattern of W 4f (B) and O 1s (C), (D) XRD pattern, (E). SEM image, (F). TEM image.

Catalytic activity of WO_3 NSs

To investigate the catalytic activity of WO_3 NSs, TMB and H_2O_2 were used as chromogenic agent and oxidant respectively, several control experiments were carried out, and the results are shown in Figure 2A. The solutions of WO_3 NSs, WO_3 NSs/TMB and WO_3 NSs/ H_2O_2 are all colorless (inset in Figure 2A) without characteristic absorption peak in the scanning range of 500 to 800 nm (curve a to c). TMB solution involving H_2O_2 merely shows a pale bluish with a weak absorption peak (curve d), indicating that TMB was slowly oxidized by H_2O_2 . While TMB solution involving H_2O_2 and WO_3 NSs results in a deep blue color with a strong absorption peak at 652 nm (curve e). The observed phenomenon is consistent with the HRP-catalyzed oxidation of TMB in the presence of H_2O_2 , demonstrating the peroxidase-like catalytic activity of WO_3 NSs.

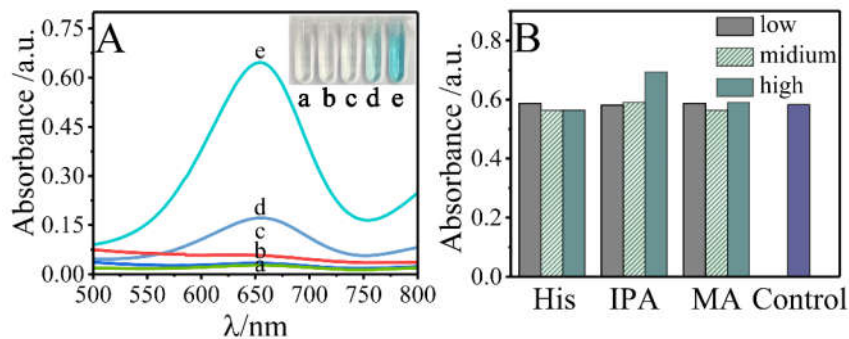


Figure 2. (A) Absorption spectra of solutions with different components. Inset: digital photos of corresponding solutions. (B) Effect of radical scavenger on the absorbance of the TMB- H_2O_2 - WO_3 NSs mixture.

Nanomaterials-based peroxidase mimetic, such as MoS₂ NSs [26], AuNPs-WS₂QDs [35], N-Fe CDs [36], and carbon quantum dots [37], can promote the decomposition of H₂O₂ to produce hydroxyl radical (•OH) intermediates, which further oxidizes TMB to blue oxidation product (oxTMB). To study the mechanism of WO₃ NSs, three •OH scavengers, including isopropyl alcohol (IPA), methyl alcohol (MA) and L-histidine (His), were added to the TMB-H₂O₂-WO₃ NSs system to evaluate the effects of WO₃ NSs on •OH generation. The absorption spectra of TMB containing H₂O₂ and WO₃ NSs in the presence and absence of •OH scavengers were monitored. As shown in Figure 2B, the concentration and type of •OH scavenger have no significant effect on the absorbance at 652 nm. These results proved that the catalytic activity of WO₃ NSs was not due to the generation of •OH. Similar to Co₃O₄-MMT NPs [38] and CoSe₂ NFs [39], whose catalytic activity is achieved by accelerating electron transfer from TMB to H₂O₂, rather than by producing •OH. Therefore, the catalytic mechanism of WO₃ NSs can be described as follows. TMB was adsorbed on WO₃ NSs surface and provided lone-pair electrons to WO₃ NSs, leading to an increase in electrons density of WO₃ NSs. Since H₂O₂ was also adsorbed on WO₃ NSs surface, an increased electron density facilitated the transfer of electrons from TMB to H₂O₂. Thus, the oxidation rate of TMB by H₂O₂ was accelerated.

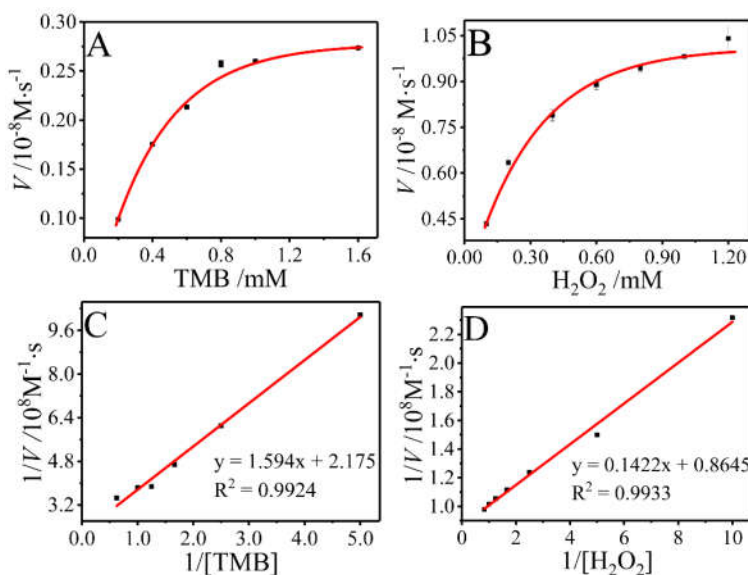


Figure 3. The steady-state kinetic and catalytic mechanism of WO₃ nanosheets. The error bar represents the standard error obtained from three repeated measurements. (A) H₂O₂ concentration is 1.0 mM, TMB concentration is different. (B) TMB concentration is 1.0 mM, H₂O₂ concentration is different. (C, D) Double reciprocal diagram of the catalytic activity of WO₃ nanosheets when the concentration of one substrate (TMB or H₂O₂) was fixed and the concentration of the other substrate was changed.

The catalytic performance of WO₃ NSs was further studied by steady-state kinetics. As displayed in Figure 3A and Figure 3B, the oxidation reaction catalyzed by WO₃ NSs follows the typical Michaelis-Menten model for both substrates TMB and H₂O₂. The Michaelis constant (K_m), which is related to the affinity of the enzyme to the substrate, were obtained from the following

equation: $1/V = (K_m/V_{max}) \times (1/[S]) + 1/V_{max}$, among them, V , V_{max} and $[S]$ represent the initial reaction velocity, the maximum initial velocity and the substrate concentration, respectively. According to Figure 3C and Figure 3D, the K_m values of WO_3 NSs to TMB and H_2O_2 were calculated to be 0.733 and 0.164 mM, respectively. It should be noted that a low K_m value implies a high catalytic activity. The K_m value of WO_3 NSs toward TMB is greater than that of HRP [19] (0.43 mM), implying that WO_3 NSs possesses a lower affinity for TMB than HRP. While the K_m value of WO_3 NSs toward H_2O_2 (3.70 mM) was lower than that of HRP, suggesting that the WO_3 NSs exhibits strong affinity for H_2O_2 [19]. Therefore, as a peroxidase-like enzyme, WO_3 NSs can be applied to the sensitive detection of H_2O_2 and its related substances.

Applications of WO_3 NSs in H_2O_2 and UA Detection

Similar to other peroxidase mimics, the catalytic activity of WO_3 NSs was also affected by external factors. To achieve the best response, we studied the influences of experimental conditions including pH value, TMB concentration, and incubation time to optimize the H_2O_2 -mediated TMB chromogenic reaction in a 30 °C water bath. As shown in Figure 4, the favorable pH, TMB concentration, and incubation time for the WO_3 NSs-catalyzed TMB oxidation are 4.5, 1.0 mM, and 50 min, respectively. Under the above experimental conditions, a simple method for colorimetric detection of H_2O_2 was established. As displayed in Figure 5A, the absorbance increases with the increase of H_2O_2 concentration, and the obvious change of solution color can be observed by the naked eye (Figure 5A inset). Furthermore, the absorbance was linear to H_2O_2 concentration in the range of 2.0-180 μ M (Figure 5B), the regression equation could be defined as $A = 0.0043C (\mu\text{M}) + 0.023$ ($R^2 = 0.991$). The limit of detection (LOD) at $3\delta/k$ (where δ is the standard deviation of 11 blank solution measurements, and k is the slope of calibration curve) for H_2O_2 was 1.34 μ M, suggesting high sensitivity for H_2O_2 detection.

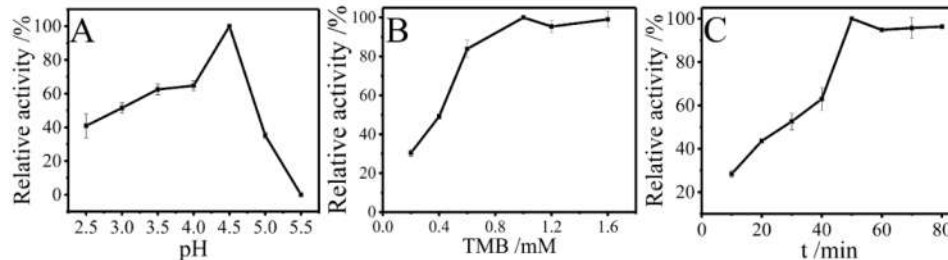


Figure 4. Effect of (A) pH value, (B) TMB concentration and (C) reaction time on the catalytic activity of the WO_3 NSs.

Under the catalysis of UAO, UA is oxidized to produce H_2O_2 quantitatively. Thus, a method for the determination of UA was further developed. As shown in Figure 5C, with the increase of UA concentration, the absorbance at 652 nm increases gradually, accompanied with obvious color change from colorless to light blue and dark blue (Figure 5C inset), indicating the possibility of visual detection of UA. As can be seen in Figure 5D, the absorbance exhibits a linear response to UA concentration over the range of 2.0 - 180 μ M, the calibration curve can be depicted as $A = 0.0046C (\mu\text{M}) + 0.0198$ ($R^2 = 0.996$). On the basis of $3\delta/k$, the LOD for UA was 1.25 μ M, which is much lower than the lowest concentration of UA in human serum (0.12 mM) [4, 5], implying a high sensitivity method for UA detection. The relative standard deviation (RSD) was 1.1% for determining 40.0 μ M UA ($n = 3$), indicating a good precision of the method. As summarized in Table 1, the developed method is superior to most of the approaches for UA detection in sensitivity or linear range.

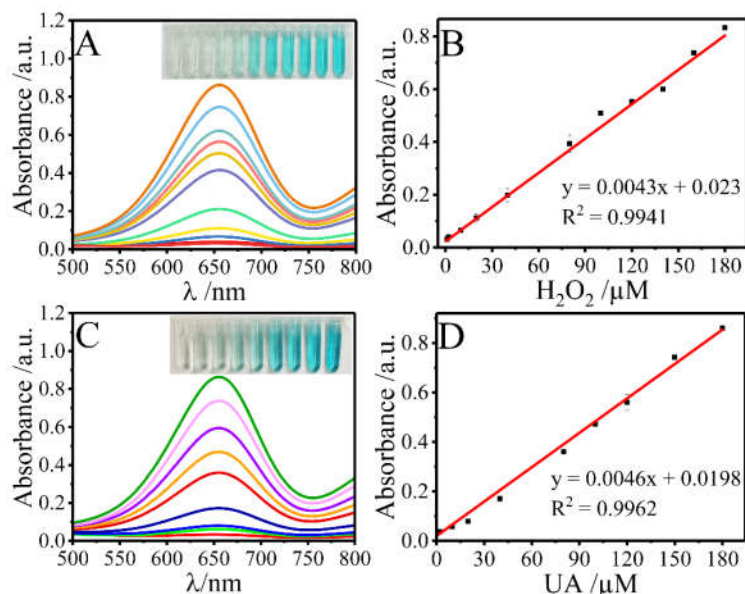


Figure 5. (A) Absorption spectra of TMB- WO_3 NSs mixture with various concentrations of H_2O_2 . Inset: digital photos of corresponding solutions. (B) The linear relation of absorbance with H_2O_2 concentration. (C) Absorption spectra of TMB- WO_3 NSs mixture with various concentrations of UA. Inset: digital photos of corresponding solutions. (D) The linear relation of absorbance with UA concentration.

Table 1. Comparison with some reported methods for the detection of uric acid.

Materials used	Method	Detection limit (μM)	Linear range (μM)	Real sample	Recovery (%)	Reference
Fe_3O_4 @fatty acid MNPs	Colorimetric	2.8	5-250	Serum	94.7-103.4	[40]
Pt@Ag NFs	Colorimetric	0.3	0.5-150	Serum	96.8-103.3	[41]
$\text{Ag}_2\text{V}_4\text{O}_{11}$ NBs	Colorimetric	0.35	1-110	*	*	[42]
Au NPs	Colorimetric	0.04	0.1-30	Urine	96.1-103.1	[43]
Fe@NCDs	Colorimetric	0.64	2-150	Urine	92.0-103.4	[44]
CoP NSs	Colorimetric	1.0	1-200	Urine	99.6-106.5	[45]
WO_3 NSs	Colorimetric	1.25	2-180	Serum	92.6-105.5	This work

The potential interferences including Glu, Cys, Gly, His, Ser, Thr, Na^+ , K^+ , and Mg^{2+} , which might coexist in serum and interfere with the determination of UA, were chosen to assess the selectivity of the method. The concentrations of UA and interferences were 0.1 and 1.0 mM, respectively. As displayed in Figure 6, the absorbance of the solution containing interference is far lower than that of UA because of the high selectivity of UAO to UA, indicating good selectivity for UA determination.

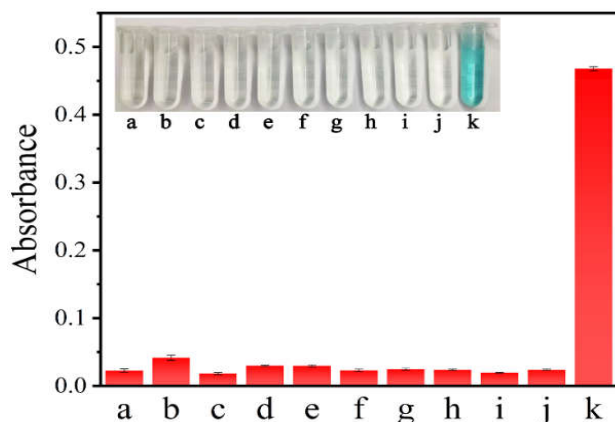


Figure 6. Selectivity evaluation for UA determination. The concentrations of UA and interferents were 0.1 and 1.0 mM respectively. (a. Glu; b. Cys; c. Gly; d. His; e. Ser; f. Thr; g. Na⁺; h. K⁺; i. K⁺; j. Mg²⁺; k. UA).

To evaluate the feasibility of the method in practical application, the concentration of UA in human serum was determined, and a standard addition method was used to verify the accuracy of the method. The results are displayed in Table 2. Considering the sample dilution (37 times) caused by the determination process, the concentration of UA in the original serum samples are 0.26 and 0.19 mM, respectively, which are within the normal range (0.12 to 0.46 mM). The recoveries of UA in serum samples ranged from 92.6% to 105.5%, and the RSD at each level was less than 3.3%, confirming an accurate and reliable method.

Table 2. Determination results of UA in human serum samples (n = 3).

Sample	Added (μM)	Found (μM)	Recovery (%)	RSD (%)
1	0	7.092	0	1.5
	20	27.65	102.8	1.0
	40	44.13	92.60	3.3
2	0	5.241	0	2.3
	40	47.46	105.5	2.7
	80	83.39	97.68	2.5

CONCLUSIONS

WO₃ NSs was prepared at room temperature, which exhibited peroxidase-like activity and could catalyze H₂O₂ to oxidize colorless TMB into blue oxTMB. Taking the advantages of the catalytic activity of WO₃ NSs and the specificity of UAO, a sensitive and selective spectrophotometric method for UA detection was developed. A good linear relationship between absorbance and UA concentration over the range of 2.0–180 μM was achieved with LOD of 1.25 μM . More importantly, the method has been used for determining UA in serum with good accuracy and precision, showing its promising potential applications.

ACKNOWLEDGEMENTS

This work was supported by the Start-up Fund for Talent Introduction of Guangxi University (A3040051025) and the Innovation Project of Guangxi Graduate Education (No. YCSW2021050).

REFERENCES

1. Huang, Z.; Xie, N.; Illes, P.; Di Virgilio, F.; Ulrich, H.; Semyanov, A.; Verkhatsky, A.; Sperlagh, B.; Yu, S.-G.; Huang, C.; Tang, Y. From purines to purinergic signalling: Molecular functions and human diseases. *Signal Transduct. Target Ther.* **2021**, *6*, 162.
2. Yang, J.; Huang, Z.; Hu, Y.; Ge, J.; Li, J.; Li, Z. A facile fluorescence assay for rapid and sensitive detection of uric acid based on carbon dots and MnO₂ nanosheets. *New J. Chem.* **2018**, *42*, 15121-15126.
3. Viridis, A.; Masi, S.; Casiglia, E.; Tikhonoff, V.; Cicero, A.F.G.; Ungar, A.; Rivasi, G.; Salvetti, M.; Barbagallo, C.M.; Bombelli, M.; Dell'Oro, R.; Bruno, B.; Lippa, L.; D'Elia, L.; Verdecchia, P.; Mallamaci, F.; Cirillo, M.; Rattazzi, M.; Cirillo, P.; Gesualdo, L.; Mazza, A.; Giannattasio, C.; Maloberti, A.; Volpe, M.; Tocci, G.; Georgiopoulos, G.; Iaccarino, G.; Nazzaro, P.; Parati, G.; Palatini, P.; Galletti, F.; Ferri, C.; Desideri, G.; Viazzi, F.; Pontremoli, R.; Muiesan, M.L.; Grassi, G.; Borghi, C. null, n., Identification of the uric acid thresholds predicting an increased total and cardiovascular mortality over 20 years. *Hypertension* **2020**, *75*, 302-308.
4. Yang, Y.; Song, Y.; Bo, X.; Min, J.; Pak, O. S.; Zhu, L.; Wang, M.; Tu, J.; Kogan, A.; Zhang, H.; Hsiai, T. K.; Li, Z.; Gao, W. A laser-engraved wearable sensor for sensitive detection of uric acid and tyrosine in sweat. *Nat. Biotechnol.* **2020**, *38*, 217-224.
5. Wang, Z.; Guo, H.; Gui, R.; Jin, H.; Xia, J.; Zhang, F. Simultaneous and selective measurement of dopamine and uric acid using glassy carbon electrodes modified with a complex of gold nanoparticles and multiwall carbon nanotubes. *Sen. Actuat. B Chem.* **2018**, *255*, 2069-2077.
6. Ahmad, M.; Faraazi, A.; Aamir, N. The effect of *Ocimum sanctum* and ledum palustre on serum uric acid level in patients suffering from gouty arthritis and hyperuricaemia. *Bull. Chem. Soc. Ethiop.* **2013**, *27*, 469-473.
7. Wang, X.-y.; Zhu, G.-b.; Cao, W.-d.; Liu, Z.-j.; Pan, C.-g.; Hu, W.-j.; Zhao, W.-y.; Sun, J.-f. A novel ratiometric fluorescent probe for the detection of uric acid in human blood based on H₂O₂-mediated fluorescence quenching of gold/silver nanoclusters. *Talanta* **2019**, *191*, 46-53.
8. Meng, F.; Yin, H.; Li, Y.; Zheng, S.; Gan, F.; Ye, G. One-step synthesis of enzyme-stabilized gold nanoclusters for fluorescent ratiometric detection of hydrogen peroxide, glucose and uric acid. *Microchem. J.* **2018**, *141*, 431-437.
9. Motshakeri, M.; Phillips, A.R.J.; Kilmartin, P.A. Application of cyclic voltammetry to analyse uric acid and reducing agents in commercial milks. *Food Chem.* **2019**, *293*, 23-31.
10. Chen, Y.; Ji, P.; Ma, G.; Song, Z.; Tang, B. Q.; Li, T. Simultaneous determination of cellular adenosine nucleotides, malondialdehyde, and uric acid using HPLC. *Biomed. Chromatogr.* **2021**, *35*, e5156.
11. Yang, M.; Wang, H.; Liu, P.; Cheng, J. A 3D electrochemical biosensor based on super-aligned carbon nanotube array for point-of-care uric acid monitoring. *Biosens. Bioelectron.* **2021**, *179*, 113082.
12. Wang, X.; Chen, S.; Tang, X.; Lin, D.; Qiu, P. Ultrasensitive detection of uric acid in serum of patients with gout by a new assay based on Pt@Ag nanoflowers. *RSC Adv.* **2019**, *9*, 36578-36585.
13. Altinkaynak, C.; Turk, M.; Ekremoglu, M.; Ozdemir, N. Peroxidase-like activity of hemoglobin-based hybrid materials against different substrates and their enhanced application for H₂O₂ detection. *Bull. Chem. Soc. Ethiop.* **2021**, *35*, 537-550.
14. Wang, L.; Yu, L.; Ge, H.; Bu, Y.; Sun, M.; Huang, D.; Wang, S. A novel reversible dual-mode probe based on amorphous carbon nanodots for the detection of mercury ion and glutathione. *Microchem. J.* **2022**, *175*, 107181.
15. Nie, Q.; Cai, Q.; Xu, H.; Qiao, Z.; Li, Z. A facile colorimetric method for highly sensitive ascorbic acid detection by using CoOOH nanosheets. *Anal. Methods* **2018**, *10*, 2623-2628.

16. Chen, C.; Zhang, S.; Zhang, C.; Li, L.; Zhu, J.; Liu, J. TMB-assembly as nanosubstrate construction colorimetric kit for highly sensitive and selective detection of H₂O₂ and monoamine oxidase-A based on Fenton reaction. *Microchem. J.* **2019**, *150*, 104177.
17. Yang, C.; Zhang, M.; Wang, W.; Wang, Y.; Tang, J. UV-Vis detection of hydrogen peroxide using horseradish peroxidase/copper phosphate hybrid nanoflowers. *Enzyme Microb. Technol.* **2020**, *140*, 109620.
18. Ocsoy, I.; Dogru, E.; Usta, S. A new generation of flowerlike horseradish peroxidases as a nanobiocatalyst for superior enzymatic activity. *Enzyme Microb. Technol.* **2015**, *75-76*, 25-29.
19. Gao, L.; Zhuang, J.; Nie, L.; Zhang, J.; Zhang, Y.; Gu, N.; Wang, T.; Feng, J.; Yang, D.; Perrett, S.; Yan, X. Intrinsic peroxidase-like activity of ferromagnetic nanoparticles. *Nat. Nanotechnol.* **2007**, *2*, 577-583.
20. Qin, X.; Yuan, C.; Shi, R.; Wang, Y. A double signal optical probe composed of carbon quantum dots and Au@Ag nanoparticles grown in situ for the high sensitivity detection of ellagic acid. *J. Mol. Liq.* **2021**, *323*, 114594.
21. Bagheri, N.; Khataee, A.; Habibi, B.; Hassanzadeh, J. Mimetic Ag nanoparticle/Zn-based MOF nanocomposite (AgNPs@ZnMOF) capped with molecularly imprinted polymer for the selective detection of patulin. *Talanta* **2018**, *179*, 710-718.
22. Xi, Z.; Wei, K.; Wang, Q.; Kim, M. J.; Sun, S.; Fung, V.; Xia, X. Nickel-platinum nanoparticles as peroxidase mimics with a record high catalytic efficiency. *J. Am. Chem. Soc.* **2021**, *143*, 2660-2664.
23. Ge, J.; Xing, K.; Geng, X.; Hu, Y.; Shen, X.; Zhang, L.; Li, Z. Human serum albumin templated MnO₂ nanosheets are oxidase mimics for colorimetric determination of hydrogen peroxide and for enzymatic determination of glucose. *Microchim. Acta* **2018**, *185*, 559.
24. Sun, J.; Li, L.; Kong, Q.; Zhang, Y.; Zhao, P.; Ge, S.; Cui, K.; Yu, J. Mimic peroxidase-transfer enhancement of photoelectrochemical aptasensing via CuO nanoflowers functionalized lab-on-paper device with a controllable fluid separator. *Biosens. Bioelectron.* **2019**, *133*, 32-38.
25. Jin, X.; Yin, W.; Ni, G.; Peng, J. Hydrogen-bonding-induced colorimetric detection of melamine based on the peroxidase activity of gelatin-coated cerium oxide nanospheres. *Anal. Methods.* **2018**, *10*, 841-847.
26. Shi, R.; He, Q.; Cheng, S.; Chen, B.; Wang, Y. Determination of glucose by using MoS₂ nanosheets as a peroxidase mimetic enzyme. *New J. Chem.* **2021**, *45*, 18048-18053.
27. Yuan, C.; Qin, X.; Xu, Y.; Jing, Q.; Shi, R.; Wang, Y. High sensitivity detection of H₂O₂ and glucose based on carbon quantum dots-catalyzed 3,3',5,5'-tetramethylbenzidine oxidation. *Microchem. J.* **2020**, *159*, 105365.
28. Zhu, Q.; Mao, H.; Li, J.; Hua, J.; Wang, J.; Yang, R.; Li, Z. A glycine-functionalized graphene quantum dots synthesized by a facile post-modification strategy for a sensitive and selective fluorescence sensor of mercury ions. *Spectrochim. Acta A Mol. Biomol. Spectrosc.* **2021**, *247*, 119090.
29. Ma, Y.; Zhao, M.; Cai, B.; Wang, W.; Ye, Z.; Huang, J. 3D graphene network@WO₃ nanowire composites: A multifunctional colorimetric and electrochemical biosensing platform. *Chem. Commun.* **2014**, *50*, 11135-11138.
30. Liu, Z.; Gong, S.; Wang, Y.; Chen, T.; Niu, Y.; Xu, Y. Recognition of the enzymatically active and inhibitive oxygenous groups on WO_{3-x} quantum dots by chemical deactivation and density functional theory calculations. *ACS Appl. Bio Mater.* **2020**, *3*, 1459-1468.
31. Li, Z.; Liu, X.; Liang, X.-H.; Zhong, J.; Guo, L.; Fu, F. Colorimetric determination of xanthine in urine based on peroxidase-like activity of WO₃ nanosheets. *Talanta* **2019**, *204*, 278-284.
32. Liang, L.; Li, K.; Xiao, C.; Fan, S.; Liu, J.; Zhang, W.; Xu, W.; Tong, W.; Liao, J.; Zhou, Y.; Ye, B.; Xie, Y. Vacancy associates-rich ultrathin nanosheets for high performance and flexible nonvolatile memory device. *J. Am. Chem. Soc.* **2015**, *137*, 3102-3108.

33. Guo, Q.; Zhao, X.; Li, Z.; Wang, D.; Nie, G. A novel solid-state electrochromic supercapacitor with high energy storage capacity and cycle stability based on poly(5-formylindole)/WO₃ honeycombed porous nanocomposites. *Chem. Eng. J.* **2020**, 384, 123370.
34. Sharma, S.; Basu, S. Highly reusable visible light active hierarchical porous WO₃/SiO₂ monolith in centimeter length scale for enhanced photocatalytic degradation of toxic pollutants. *Sep. Purif. Technol.* **2020**, 231, 115916.
35. Vinita; Nirala, N.R.; Prakash, R. Facile and selective colorimetric assay of choline based on AuNPs-WS₂QDs as a peroxidase mimic. *Microchem. J.* **2021**, 167, 106312.
36. Yue, G.; Li, S.; Liu, W.; Ding, F.; Zou, P.; Wang, X.; Zhao, Q.; Rao, H. Ratiometric fluorescence based on silver clusters and N, Fe doped carbon dots for determination of H₂O₂ and UA: N, Fe doped carbon dots as mimetic peroxidase. *Sen. Actuat. B Chem.* **2019**, 287, 408-415.
37. Shu X.; Wang D.; Yuan C.; Qin X.; Wang Y. Colorimetric determination of sarcosine with carbon quantum dots as mimetic peroxidase. *Chem. J. Chinese Universities* **2021**, 42, 1761-1767.
38. Zhu, X.; Chen, W.; Wu, K.; Li, H.; Fu, M.; Liu, Q.; Zhang, X. A colorimetric sensor of H₂O₂ based on Co₃O₄-montmorillonite nanocomposites with peroxidase activity. *New J. Chem.* **2018**, 42, 1501-1509.
39. Warkhade, S.K.; Singh, R.P.; Das, R.S.; Gaikwad, G.S.; Zodape, S.P.; Pratap, U.R.; Maldhure, A.; Wankhade, A.V. CoSe₂ nanoflakes: An artificial nanoenzyme with excellent peroxidase like activity. *Inorg. Chem. Commun.* **2021**, 126, 108461.
40. Wen, J.; Yun, Z.; Zhili, C.; Yang, Y. Peroxidase-like activity of Fe₃O₄@fatty acid-nanoparticles and their application for the detection of uric acid. *New J. Chem.* **2020**, 44, 18608-18615.
41. Wang, X.; Chen, S.; Tang, X.; Lin, D.; Qiu, P. Ultrasensitive detection of uric acid in serum of patients with gout by a new assay based on Pt@Ag nanoflowers. *RSC Adv.* **2019**, 9, 36578-36585.
42. Sun, L.; Shen, H.; Zheng, L.; Gao, P.; Xiang, Z. Colorimetric detection of uric acid based on peroxidase-like activity of Ag₂V₄O₁₁ nanobelts. *J. Electron. Mater.* **2021**, 50, 3907-3915.
43. Li, F.; He, T.; Wu, S.; Peng, Z.; Qiu, P.; Tang, X. Visual and colorimetric detection of uric acid in human serum and urine using chitosan stabilized gold nanoparticles. *Microchem. J.* **2021**, 164, 105987.
44. Liang, C.; Lan, Y.; Sun, Z.; Zhou, L.; Li, Y.; Liang, X.; Qin, X. Synthesis of carbon quantum dots with iron and nitrogen from *Passiflora edulis* and their peroxidase-mimicking activity for colorimetric determination of uric acid. *Microchim. Acta* **2020**, 187, 405.
45. He, Y.; Qi, F.; Niu, X.; Zhang, W.; Zhang, X.; Pan, J. Uricase-free on-demand colorimetric biosensing of uric acid enabled by integrated CoP nanosheet arrays as a monolithic peroxidase mimic. *Anal. Chim. Acta* **2018**, 1021, 113-120.